









RESEARCH ARTICLE

Holdemanella biformis improves glucose tolerance and regulates GLP-1 signaling in obese mice

Marina Romani-Pérez¹  | Inmaculada López-Almela¹  | Clara Bullich-Vilarrubias¹  |
 Lola Rueda-Ruzafa²  | Eva M. Gómez Del Pulgar¹  | Alfonso Benítez-Páez¹  |
 Gerhard Liebisch³ | José Antonio Lamas²  | Yolanda Sanz¹ 

¹Microbial Ecology, Nutrition and Health Research Unit, Institute of Agrochemistry and Food Technology, National Research Council (IATA-CSIC), Valencia, Spain

²Laboratory of Neuroscience, Biomedical Research Center (CINBIO), University of Vigo, Vigo, Spain

³Institute of Clinical Chemistry and Laboratory Medicine, University of Regensburg, Regensburg, Germany

Correspondence

Marina Romani-Pérez, Microbial Ecology, Nutrition and Health Research Unit, Institute of Agrochemistry and Food Technology, National Research Council (IATA-CSIC), Valencia 46980, Spain.
 Email: marina.romani@iata.csic.es

Funding information

European Union Horizon 2020 research and innovation program, Grant/Award Number: 797297; European Union 7th Framework Program, Grant/Award Number: 613979; Spanish Ministry of Science and Innovation, Grant/Award Number: AGL2017-88801-P

Abstract

Impaired glucose homeostasis in obesity is mitigated by enhancing the glucoregulatory actions of glucagon-like peptide 1 (GLP-1), and thus, strategies that improve GLP-1 sensitivity and secretion have therapeutic potential for the treatment of type 2 diabetes. This study shows that *Holdemanella biformis*, isolated from the feces of a metabolically healthy volunteer, ameliorates hyperglycemia, improves oral glucose tolerance and restores gluconeogenesis and insulin signaling in the liver of obese mice. These effects were associated with the ability of *H. biformis* to restore GLP-1 levels, enhancing GLP-1 neural signaling in the proximal and distal small intestine and GLP-1 sensitivity of vagal sensory neurons, and to modify the cecal abundance of unsaturated fatty acids and the bacterial species associated with metabolic health. Our findings overall suggest the potential use of *H. biformis* in the management of type 2 diabetes in obesity to optimize the sensitivity and function of the GLP-1 system, through direct and indirect mechanisms.

KEYWORDS

glucagon-like peptide 1, gut microbiota, *Holdemanella biformis*, obesity, type 2 diabetes, vagal afferent neurons

Abbreviations: *Acs13*, long-chain acyl-CoA synthetase; *Agrp*, agouti-related peptide; AP, action potential; *Cart*, cocaine and amphetamine regulated transcript; CD, control diet; *Cldn3*, claudin 3; DIO, diet-induced obesity; DPP-4, dipeptidyl peptidase-4; *G6pase*, glucose-6-phosphatase; GLP-1, glucagon like peptide-1; *Glp1r*, GLP-1 receptor; GLP-2, glucagon like peptide-2; HFHSD, high fat high sugar diet; LCFAs, long chain fatty acids; LC-MS/MS, liquid chromatography–mass spectrometry; *Lyz1*, lysozyme 1; MS (GC-MS), gas chromatography–mass spectrometry; MUFAs, monounsaturated fatty acids; NG, nodose ganglion; nNOS, nitric oxide synthase; *Npy*, neuropeptide Y; *Ocln*, occludin; OGTT, oral glucose tolerance test; *Pck1*, phosphoenolpyruvate carboxykinase 1; *Pla2g2a*, phospholipase A2 group IIA; *Pomc*, proopiomelanocortin; PUFAs, polyunsaturated fatty acids; PYY, peptide tyrosine tyrosine; *Reg3γ*, regenerating islet-derived protein 3 gamma; RMP, resting membrane potential; *Rpl19*, ribosomal protein 19; SCFAs, short chain fatty acids; T2D, type 2 diabetes; *Tcf4*, transcription factor 4.

Marina Romani-Pérez and Inmaculada López-Almela equally contributed to this study.

This is an open access article under the terms of the Creative Commons Attribution-NonCommercial-NoDerivs License, which permits use and distribution in any medium, provided the original work is properly cited, the use is non-commercial and no modifications or adaptations are made.

© 2021 The Authors. *The FASEB Journal* published by Wiley Periodicals LLC on behalf of Federation of American Societies for Experimental Biology

1 | INTRODUCTION

The increasing worldwide prevalence of obesity and its associated disorders are a major global health challenge. Growing evidence supports a role for the gut microbiota in insulin resistance and in the onset of type 2 diabetes (T2D) in obesity. For example, human observational studies have shown that specific perturbation in the structure and/or function of gut microbiota correlates with impaired metabolic health.^{1,2} Additionally, transplantation of gut microbiota from twins discordant for obesity to mice replicates the donor metabolic phenotype, demonstrating its causality in metabolic diseases.³ Western diets (high in fats and simple sugars) can trigger gut microbiota alteration,^{4,5} which might disturb the interactions between microbiota-derived metabolites and/or subcellular bacterial components and the immune, endocrine, and/or neural pathways that control host metabolism.^{6,7} Indeed, it has been shown that Western diet-associated microbiota has a negative impact on intestinal immunity^{8,9} and impairs the functionality of gut-derived hormones such as glucagon-like peptide-1 (GLP-1),^{10,11} ultimately affecting energy homeostasis. This evidence also supports the notion that gut microbiota can be manipulated to restore the misconfigured signaling pathways between the gut and distant organs and systems and, thus, beneficially influence metabolic phenotypes.

Given the known benefits of GLP-1, including its insulinotropic effects in the pancreas and improving peripheral insulin sensitivity, several GLP-1-based therapies have been developed to counteract the development of obesity-induced glucose intolerance.¹² GLP-1 and its mimetics modulate insulin and glucagon secretion in distal β and α pancreatic cells, respectively, via endocrine routes, and can stimulate intestinal vagal afferents in a paracrine manner, thereby indirectly controlling glucose tolerance through central nervous system-mediated metabolic circuits.^{13,14} By-products of microbiota metabolism or bacterial structural components might affect the function of GLP-1-secreting enteroendocrine L cells¹⁵⁻¹⁷ and thus influence both endocrine- and neuroparacrine-mediated GLP-1 actions. Indeed, a recent study suggests that the commensal gut microbiota is necessary to adequately maintain the sensitivity of GLP-1-mediated paracrine signaling through the activation of vagal afferent fibers in the intestine.¹⁰ Accordingly, there is growing interest in the development of microbiota-based therapies to potentiate the activity of antidiabetic drugs targeting GLP-1 signaling.¹⁸ In this line, several studies have attempted to identify specific gut bacteria of lean subjects that might contribute to restore the metabolic signaling that often goes awry in obesity.¹⁹⁻²¹ Some of the bacteria investigated so far, such as *Akkermansia muciniphila* or *Bacteroides* spp., have demonstrated beneficial effects on glucose homeostasis in preclinical studies of obesity.²²⁻²⁴ Mechanistic studies have

established that these effects can be partly attributed to the ability of the bacteria to reduce intestinal inflammation and protect against the gut barrier disruption associated with obesity.^{22,24,25} Emerging investigations reveal that gut microbiota also impacts on host energy homeostasis by influencing on the enteroendocrine system²⁶ inducing regional-specific effects on the enteroendocrine cells.²⁷ Nonetheless, further investigations are required to identify key intestinal bacteria acting on the enteroendocrine system and, thereby, regulating host metabolism.

Holdemanella biformis (formerly *Eubacterium biformis*) is a human gut bacterium^{28,29} that through the release of short chain fatty acids (SCFAs) and the long chain fatty acid (LCFA) 3-hydroxyoctadecaenoic is reported to induce antitumorigenesis and antiinflammatory effects.^{30,31} In addition, this bacterial species can potentially modulate the enteroendocrine cells since SCFAs as well as certain LCFAs act as a GLP-1 secretagogues.^{32,33} Here, we postulate that the intestinal bacterium *H. biformis*, through the modulation of immune and/or neuroendocrine routes of communications with the host, has a beneficial impact on obesity. To test this hypothesis, we used a diet-induced obese (DIO) mouse model to explore (1) the effects of a strain of *H. biformis*, isolated from a metabolically healthy human subject, on energy homeostasis; (2) whether its benefits are mediated through immune-regulatory mechanisms or by stimulating the secretion of gastrointestinal hormones from L cells (PYY, GLP-1 and GLP-2) and/or signaling via endocrine or paracrine routes through neural pathways of the gut-brain axis; and (3) whether the metabolic effects are related to gut microbiota changes, analyzed by 16S rRNA gene sequencing and fecal metabolomics using liquid chromatography-tandem mass spectrometry (LC-MS/MS) and gas chromatography-MS (GC-MS).

2 | MATERIAL AND METHODS

2.1 | Isolation and cultivation of *Holdemanella biformis*

Feces from healthy volunteers were homogenized in PBS containing cysteine (0.05%) and NaCl (130 mM) (Stomacher Lab-Blender 400, Seward Medical, London, UK), inoculated at 1:5 proportion in intestinal bacterial medium (0.5% starch; 0.4% mucin; 0.3% casein; 0.2% peptone, NaHCO₃, pectin, xylan and wheat bran extract; 0.1% arabinogalactans, arabic gum and inulin; 0.05% cysteine; 0.01% NaCl; 0.005% hemin; 0.004% K₂HPO₄; 0.001% CaCl₂ and MgSO₄; and 0.0001% menadione), and fermented for 24 hours in an anaerobic chamber (Whitley DG250 Workstation, Don Whitley Scientific Ltd., Shipley, UK) with stirring and pH control (6.9-7.0).

Serial dilutions of fermented feces were plated in fastidious anaerobe agar media plates containing 0.5% defibrinated

sheep blood and filtered (0.22 μm) and fermented intestinal bacteria medium, used as a nutritional supplement (0.1 mL of medium per agar plate). Dilutions were then incubated at 37°C for 72 hours in an anaerobic chamber. Bacterial DNA of each isolate (more than 200 colonies) was obtained by incubating pure colonies suspended in sterile PBS treated at 100°C for 10 minutes. The identification of each isolate was performed by polymerase chain reaction (PCR) amplification of the 16S rRNA gene using the primers 27f (5'-AGAGTTTGATCCTGGCTCAG-3') and 1401r (5'-CGGTGTGTACAAGACCC-3'). PCR products were cleaned with the Illustra GFX PCR DNA and Gel Band Purification Kits (GE Healthcare, Madison, WI) and sequenced by Sanger technology in an ABI 3730XL sequencer (Stabvida, Portugal). Using the BLASTn algorithm and the NCBI database, we identified one of the colonies as *Holdemanella biformis*, with an identity of 98%, with others belonging to this specie. The strain was further grown in chopped meat medium supplemented with 0.1% Tween80 (according to DSMZ culture collection recommendations). For in vivo experiments, bacterial cells were harvested by centrifugation (6000 g for 10 minutes) from broth cultures and washed in PBS (130-mM sodium chloride, 10 -mM sodium phosphate, and pH 7.4). Bacterial cells were then resuspended in 10% sterile skimmed milk for animal trials (Scharlau, Spain). Aliquots were immediately frozen in liquid nitrogen and stored at -80°C until use. After freezing and thawing, live cell numbers were measured using BD Trucount Tubes (BD) in a BD LSRFortessa (Becton Dickinson, Franklin Lakes, NJ) flow cytometer running FACS Diva software v.7.0.

2.2 | Mice and diets

Adult C57BL/6 mice (6-8 weeks old, Charles River, Saint Germain, Nuelles, France) were housed under controlled conditions of temperature (23°C), light/dark cycle of 12 hours, and relative humidity (40%–50%). Mice were fed for 13 weeks with a high-fat/high-sugar diet (HFHSD, D12451) containing 45% of kcal from fat and 17% of kcal from sucrose, or with a control diet (CD, D12450K), without sucrose and with 10% kcal from fat (Research Diets, Inc, Brogaarden, Denmark). HFHSD-fed mice received a daily oral dose of *H. biformis* (5×10^8 cells in 10% skimmed milk, $n = 10$) or vehicle (10% skimmed milk, $n = 10$), while CD-fed mice received only vehicle ($n = 9$). Thirteen weeks after the intervention, blood obtained by cardiac puncture from isofluorane-anesthetized mice was collected into microfuge tubes containing K3 EDTA (Sarstedt, Nümbrecht Germany) and immediately centrifuged to obtain plasma and stored at -80°C until use. Mice were then sacrificed by cervical dislocation for sampling collection, including duodenum,

ileum and colon (2 cm), liver, brain, cecal content, and feces, which were all immediately frozen until use. All experimental procedures were performed in accordance with European Union 2010/63/UE and Spanish RD53/2013 guidelines and approved by the local ethics committee (Animal Production Section, Central Service of Support to Research [SCSIE], University of Valencia, Spain) and authorized by Dirección General de Agricultura, Ganadería y Pesca (Generalitat Valenciana; approval ID 2017/VSC/PEA/00015).

2.3 | Flow cytometry

Small intestine was cleaned with cold PBS, opened longitudinally, and cut into small pieces. For the isolation of the epithelium, tissue was incubated twice in Hank's balanced salt solution (HBSS) with calcium and magnesium (ThermoFisher Scientific, Massachusetts, USA) containing 5-mM EDTA (Scharlab), 1-mM DTT, 100- $\mu\text{g}/\text{mL}$ streptomycin, and 100-U/mL penicillin (Merck, Darmstadt, Germany) in orbital shaker for 30 minutes at 37°C. Cells from the epithelium were collected by filtrating supernatant fractions with 100- μm nylon cell strainers that were then centrifuged to harvest cell suspensions. Epithelium isolated cells in FACS buffer (PBS with BSA 0.5%) were incubated with different immune markers during 30 minutes at 4°C in darkness. Natural (CD45+ CD2+ CD5+) and induced (CD45+ CD2- CD5-) intraepithelial lymphocytes (IEL) were determined by phycoerythrin (PE)-conjugated anti-CD45, allophycocyanin (APC)-conjugated anti-CD2, and PE-Vio770-conjugated anti-CD5 (Miltenyi Biotec, Bergisch Gladbach, Germany) antibodies. Innate lymphoid cells type 1 (ILC1: CD90+ CD127+ LIN-Tbet+IFN γ +) were labeled by VioBlue-conjugated anti-CD90, Pe-Vio770-conjugated anti-CD127 (Miltenyi Biotec, Bergisch Gladbach, Germany), PerCP-CyTM5.5-conjugated antil lineage antibody cocktail (LIN) (BD-Bioscience, USA), phycoerythrin (PE)-conjugated anti-Tbet, and allophycocyanin (APC)-conjugated anti-IFN γ (Miltenyi Biotec, Bergisch Gladbach, Germany) antibodies. Staining cells were permeabilized and fixed (fixation/permeabilization solution kit, BD Bioscience, USA) when intracellular markers were required. Data acquisition and analysis were performed using a BD LSRFortessa (Becton Dickinson, USA) flow cytometer operated by FACS Diva software v.7.0 (BD Biosciences, USA).

2.4 | Oral glucose tolerance test and blood metabolic parameters

After 8 and 10 weeks of HFHSD feeding, blood from the saphenous vein was used to measure baseline fasting blood glucose in 4-h food-deprived mice using the Contour XT glucometer (Bayer, Germany). An oral glucose tolerance test

(OGTT) was conducted at week 10 of DIO by measuring glycemia at 0, 15, 30, 60, and 120 minutes after administering an oral glucose load (2 g/kg). At week 13, metabolic parameters including triglycerides, cholesterol, and hormones such as insulin, the active isoform of glucagon-like peptide-1 (GLP-1), GLP-2, and peptide YY (PYY) were analyzed in plasma obtained by blood centrifugation at 600 g for 15 minutes at 4°C. Dipeptidyl-peptidase (DPP)-4 inhibitor (Merck, Germany) was added into blood collecting tubes to prevent GLP-1 degradation. The Free Fatty acid kit (Sigma-Aldrich), Triglyceride Colorimetric Assay Kit (Elabscience, Houston, TX), and the Cholesterol Liquid Kit (Química Clínica Aplicada SA, Spain) were employed to measure free fatty acids, triglycerides, and cholesterol, respectively. Insulin, PYY and GLP-1 were quantified using the multiplex assay Milliplex MAP Mouse Metabolic Hormone Magnetic Bead Panel kit (Merck, Darmstadt, Germany) on a Luminex 200 platform (Luminex, Austin, TX). GLP-2 was measured using EIA kit for GLP-2 (Abyntek Biopharma, Vizcaya, Spain). Colorimetric signals from triglycerides, cholesterol and GLP-2 analysis were measured in a Thermo Scientific MultiSkan 1500 Reader (Thermo Fisher Scientific, Rockford, IL).

2.5 | Metabolites in liver

Hepatic glycogen, acetyl-CoA, and glucose-6-phosphatase activity were quantified in the total homogenized liver using a Glycogen Assay Kit, Acetyl-Coenzyme A Assay Kit (Sigma-Aldrich), and Glucose-6-phosphatase (G6P) Assay kit (Elabscience), respectively.

2.6 | RT-qPCR

Total RNA from duodenum, ileum, colon, liver, and hypothalamus was isolated using TRIsure lysis reagent (Bioline, London, UK). A total of 2 µg of RNA, quantified using a NanoDrop ND-1000 spectrophotometer (Thermo Fisher Scientific), was reverse transcribed using a High-Capacity cDNA Reverse Transcription Kit (Thermo Fisher Scientific) and incubated for 10 minutes at 25°C, 120 minutes at 37°C, and 5 minutes at 85°C, with a final cooling step at 4°C. cDNA amplification was conducted with the LightCycler 480 SYBR Green I Master Mix (Roche, Basel, Switzerland) containing an appropriate primer pair of each gene [*Acs13*, *Agrp*, *Cldn3*, *Cart*, *Gpr40*, *Gpr43*, *Gpr41*, *Gpr119*, *Glp-1r*, *G6pase*, *Ki67*, *Lyz1*, *Npy*, *nNOS*, *Ocln*, *Peripherin*, *Pck1*, *Pla2g2a*, *Proglucagon*, *Pomc*, *Pyy*, *Reg3γ* and *Tfc4* (Isogen Life Science, Utrecht, The Netherlands) and *Gpr120* and *Glp-1r* (Sigma-Aldrich)]. Ribosomal protein L19 (*Rpl19*) was used as housekeeping gene (primer pair sequences are detailed in Table S1). qPCR reactions were performed using

a LightCycler 480 Instrument (Roche) and variation of cDNA abundance was calculated according to the $2^{-\Delta\Delta Ct}$ method and represented as fold change expression relative to the control group.

2.7 | Western blotting

Total proteins from liver were extracted from the organic phase obtained using the TRIsureTM RNA Isolation Reagent (Bioline). In total, 5 µg of denatured proteins, quantified using Bradford's method, was separated by SDS-PAGE electrophoresis and transferred onto polyvinylidene difluoride (PVDF) membranes (Thermo Fisher Scientific). Membranes were incubated overnight at 4°C with 1:1000 dilution of phospho-Akt (Ser473), Akt, and β-actin primary antibodies (Cell Signaling Technology, Beverly, MA) followed by a 1-h incubation at RT with antirabbit IgG, HRP-linked antibody at 1:5000 (Cell Signaling Technology). Chemiluminescence signals were enhanced by adding the ECL reagent (SuperSignal West Dura Extended Duration Substrate, Thermo Fisher Scientific) and quantified using ImageJ 1.8 software.

2.8 | Fecal metabolomics

Cecal content was homogenized by bead beating in 70% isopropanol.³⁴ SCFAs were quantified by liquid chromatography coupled to tandem mass spectrometry (LC-MS/MS) upon derivatization to 3-nitrophenylhydrazones.³⁴ Concentrations of total fatty acids (LCFA) were determined by GC-MS after derivatization to fatty acid methyl esters (FAMES).³⁵

2.9 | Fecal microbiota analysis

Fecal DNA was extracted using the QIAamp PowerFecal DNA Kit (Qiagen, Hilden, Germany). Bead beating was carried out in a Mini-Bead Beater apparatus (BioSpec Products, Bartlesville, OK) with two cycles of shaking during 1 minute and incubation on ice between cycles. The fecal DNA concentration was measured using a Nanodrop spectrophotometer, and an aliquot of every sample was prepared at 10 ng/µL with nuclease-free water for PCR. The V3-V4 hypervariable regions of the 16S ribosomal ribonucleic acid (rRNA) gene were amplified using 10-ng DNA (1-µL diluted aliquot) and 25 PCR cycles consisting of the following steps: 95°C for 20 seconds, 55°C for 20 seconds, and 72°C for 20 seconds. Phusion High-Fidelity Taq Polymerase (Thermo Fisher Scientific), 6-mer barcoded primers, S-D-Bact-0341-b-S-17 (TAGCCTACGGGNGGCWGCAG), and S-D-Bact-0785-a-A-21 (ACTGACTACHVGGGTATCTAATCC) that target a wide repertoire of bacterial 16S rRNA genes³⁶ were used for

PCR. Dual barcoded PCR products of ~500 bp were purified from triplicate reactions with the Illustra GFX PCR DNA and Gel Band Purification Kit (GE Healthcare, Bucks, UK) and quantified using the Qubit 3.0 and the Qubit dsDNA HS Assay Kit (Thermo Fisher Scientific). The samples were multiplexed in one sequencing run by combining equimolar quantities of amplicon DNA (~50 ng per sample) and sequenced in one lane of the Illumina MiSeq platform with 2 × 300 PE configuration (Eurofins Genomics GmbH, Ebersberg, Germany). Raw data were delivered in fastq files, and pair ends with quality filtering were assembled using Flash software.³⁷ Sample demultiplexing was carried out using sequence information from the respective DNA barcodes and Mothur v1.39.5 suite of analysis.^{38,39} After assembly and barcodes/primers removal, the sequences were processed for chimera removal using the Uchime algorithm⁴⁰ and the SILVA reference set of 16S sequences (Release 128).⁴¹ Alpha diversity descriptors (Chao's richness, Simpson's evenness and Simpson's reciprocal index) were computed using QIIME v1.9.1³⁸ and a rarefied subset of 35 000 sequences per sample, randomly selected after multiple shuffling (10 000×) from of the original dataset. The information derived from the Operational Taxonomic Unit (OTU)-picking approach by using the rarefied set of sequences and the uclust algorithm, implemented in USEARCH v8.0.1623,⁴² was also used to evaluate the beta-diversity with the respective algorithms implemented in QIIME v1.9.1. The evaluation of the community structure across the sample groups was assisted by Principal Coordinate Analysis (PCoA) from Bray–Curtis dissimilarity indexes retrieved from sample pairwise comparisons. The taxonomy identification of OTUs was based on SILVA database and retrieved from SINA aligner.⁴³ Tracing and quantification of *H. biformis* colonization of gut mice were achieved as follows: OTUs classified as *Holdemanella* and *Faecalibaculum* (a mice symbiont homolog to *Holdemanella*³⁰) at the genus level were aligned with PyNAST algorithm implemented in QIIME and the SILVA aligned reference database, whereas the tree topology reconstruction was completed with the FastTree algorithm⁴⁴ using the generalized time-reversible (GTR) model and gamma-based likelihood. Phylogenetic tree was drawn with iTOL webserver.⁴⁵

2.10 | *Proglucagon* expression and GLP-1 secretion in human HuTu-80 cells

HuTu-80 cells (ATCC HTB-40, Manassas, VA) were cultured in Eagle's Minimum Essential Medium (EMEM; Gibco-Invitrogen, Carlsbad, CA), supplemented with 10% fetal bovine serum (FBS, Capricorn Scientific, Germany) and streptomycin (100 µg/mL), penicillin (100 IU/mL) (Sigma-Aldrich, Madrid, Spain) in a 5% CO₂ atmosphere at 37°C. For the analysis of *proglucagon* expression and GLP-1

secretion, HuTu-80 cells were seeded into 24-well plates (1 × 10⁵ cells per well) 24 hours prior to the experiment. On the day of the experiment, cells were washed twice with 500 µL of glucose-free Krebs–Ringer buffer containing 120-mM NaCl, 5-mM KCl, 2-mM CaCl₂, 1-mM MgCl₂, 22-mM NaHCO₃, and 0.1-mM DiprotinA (Merck) for 10 minutes at 37°C in a 5% CO₂ incubator. Cells were then incubated for 3 or 6 hours either with *H. biformis* (1:100 cell/bacteria proportion) or with GLP-1 secretion enhancers [ie, forskolin, 10 µM or phorbol 12-myristate 13-acetate (PMA), 200 nM; Sigma-Aldrich] used as positive controls or PBS used as negative control. Cells and supernatants were separated by centrifugation and then collected and frozen until used. Total RNA, isolated using the NucleoSpin RNA Kit (MACHEREY-NAGEL, Düren, Germany) was retrotranscribed to measure *proglucagon* gene expression by qPCR which was normalized by Rpl19 expression as housekeeping (primer sequences detailed in Table S1). Total GLP-1 protein levels in supernatants were quantified using Milliplex MAP Human Metabolic Magnetic Bead Panel (Merck) on a Luminex 200 platform (Luminex).

2.11 | Primary culture of nodose ganglion neurons

Swiss CD-1 mice were anesthetized by CO₂ inhalation and sacrificed by decapitation. The nodose ganglion (NG) was isolated and cultured as described.⁴⁶ Briefly, the NG was bilaterally isolated from the ventral neck and incubated with collagenase (2.5 mg/mL) in Hank's Balanced Salt Solution (HBSS) with 1% HEPES (Sigma-Aldrich) for 15 minutes, followed by 30-min incubation with trypsin (1 mg/mL, Sigma-Aldrich) in HBSS-1% HEPES. The NG was then mechanically disaggregated, centrifuged (500 g, 3 minutes at 22°C) and seeded onto laminin-precoated culture dishes containing L15 medium with sodium bicarbonate (24 mM), FBS (10%), glucose (38 mM), streptomycin (100 µg/mL), penicillin (100 IU/mL), and nerve growth factor (50 ng/mL) (Sigma-Aldrich). Neurons were maintained at 37°C/5% CO₂/95% O₂ for 24 hours before electrophysiological recordings or Ca²⁺ imaging.

2.12 | Electrophysiological recordings in primary cultures of nodose ganglion neurons

Resting membrane potential (RMP) and action potential (AP) firing were measured in NG neurons using perforated whole-cell patch-clamp recordings. Cells were maintained in a continuous perfusion (10 mL/min) of extracellular solution containing: 140-mM NaCl, KCl 3 mM, MgCl₂ 1 mM, CaCl₂ 2 mM, D-glucose 10 mM, HEPES 10 mM, gassed

with O₂; pH was adjusted to 7.2 with Tris. The pipette solution contained the following: K-acetate 90 mM, KCl 20 mM, MgCl₂ 3 mM, CaCl₂ 1 mM, EGTA 3 mM, HEPES 40 mM, with pH adjusted to 7.2 using NaOH. Pipette solution also contained amphotericin-B (75 µg/mL), and tips were fire-polished to give a resistance of 4–6 MΩ. Experiments were performed in current clamp mode (holding at –60 mV) using an Axopatch 200B (Axon Instruments Inc, Burlingame, CA) amplifier. To study AP firing, currents from 25 to 175 pA with increases of 25 pA were sequentially injected. First, the effect of *H. biformis* on RMP and firing was studied in extracellular solution containing PBS or 2 × 10⁶ cells/ml *H. biformis*. Similarly, the potential GLP-1 effect was studied comparing solutions containing PBS or 100-nM GLP-1. Finally, NG neurons were perfused with PBS or with 2 × 10⁶ cells/ml of *H. biformis* followed by 100-nM GLP-1. In all cases, neurons were manually clamped at –60 mV and the depolarizing effect of *H. biformis* corrected before adding GLP-1. For the study of APs only adapting neurons were considered.

2.13 | Fluorescent Ca²⁺ imaging

NG neurons were seeded onto µ-slide chamber slides (ibiTreat; Sanilabo SL, Valencia, Spain) and loaded for 45 minutes at 37°C with Fluo-4 AM loading solution (Thermo Fisher Scientific). Fluo-4 AM loading solution was removed, and medium was added again after one wash with HBSS-1% HEPES. Ca²⁺ responses were assessed by monitoring Fluo-4 dye fluorescence (excitation: 494 nm, emission: 506 nm) using a 40× magnification oil objective in an Olympus FV1000 confocal laser scanning microscope (*Central Service for Experimental Research of University of Valencia*) equipped with a heated stage maintained at 37°C/5% CO₂. Time-lapse images were captured every second for 300 seconds after addition of *H. biformis* (2 × 10⁶ cells/mL) or every second for 30 seconds after addition of PBS. Ca²⁺-mediated fluorescence intensities of cells were determined as mean gray values using ImageJ1.8.0 (www.imagej.nih.gov). For each timepoint, the relative fluorescence intensity ($\Delta F/F_0$) was calculated as fluorescence intensity after bacteria stimulation minus fluorescence intensity at baseline (ΔF) divided by the fluorescence intensity at baseline (F_0) and expressed as percentage. All fluorescence intensity values had been previously corrected by subtracting the background fluorescence intensity from the cell fluorescence intensity.

2.14 | Quantification and statistical analysis

Statistics of Figures 1–3, 6, and 7 and Figures S1, S3, and S4 were performed using GraphPad Prism 5. Data were

analyzed through one-way analysis of variance (ANOVA) followed by the Tukey post hoc test to compare the three experimental groups (CD-Veh, HFHSD-Veh, and HFHSD-*H. bif*). Two-way ANOVA followed by the Bonferroni post hoc test was used to examine the interaction between two independent variables. The differences between two matched groups were analyzed with paired *t* test. Correlations were calculated using Pearson's test. Differences were considered significant at $P < .05$. All data are shown as mean ± standard error of the mean (SEM). Statistical assessment of microbiota data (Figures 4, 5, and S2) was performed in R v3.5 and supported by application of nonparametric methods such as Kruskal–Wallis and pairwise Wilcoxon Rank Sum test with the Benjamini–Hochberg post hoc correction followed by linear discriminant analysis (LDA).⁴⁷ The relationships between microbiota changes and the different experimental mouse groups were established for those OTUs exhibiting an LDA score ≥3.0. A permutation-based analysis (Permanova) was applied to evaluate changes in the microbial structure. Correlation among the OTUs abundance (top 166 OTUs) and fatty acids concentration was performed estimating the rank-based Kendall's tau (τ) parameter with Benjamini–Hochberg post hoc correction.

3 | RESULTS

3.1 | *Holdemanella biformis* improves glucose homeostasis and restores the plasma levels of PYY and GLP-1 in DIO mice independent of obesity

Compared with mice fed a CD, both body weight gain throughout the 13-week experimental period and end of study plasma cholesterol levels were markedly increased in untreated and *H. biformis*-treated mice on HFHSD to induce DIO, whereas triglycerides and free fatty acid levels in plasma and caloric intake were unaffected (data not shown). After 10 weeks of HFHSD, basal glycemia was increased (Figure 1A) and oral glucose tolerance was impaired (Figure 1B). DIO mice administered *H. biformis* showed reduced basal glycemia reaching values similar to those of CD mice and improved glucose clearance in response to an oral glucose load, as revealed by a partial restoration of glucose clearance over time and a reduction of the AUC compared with untreated DIO mice (Figure 1B), independent of obesity. *H. biformis* intervention increased the levels of the gastrointestinal hormones PYY and GLP-1 to CD values that were reduced in untreated DIO mice (Figure 1C,D), but the bacterium did not restore the HFHSD-induced hyperinsulinemia (data not shown).

The mRNA levels of *pyy* and *proglucagon*, the precursor of GLP-1, were increased by *H. biformis* administration in the colon (Figure 1E) but not in the ileum of DIO mice (data

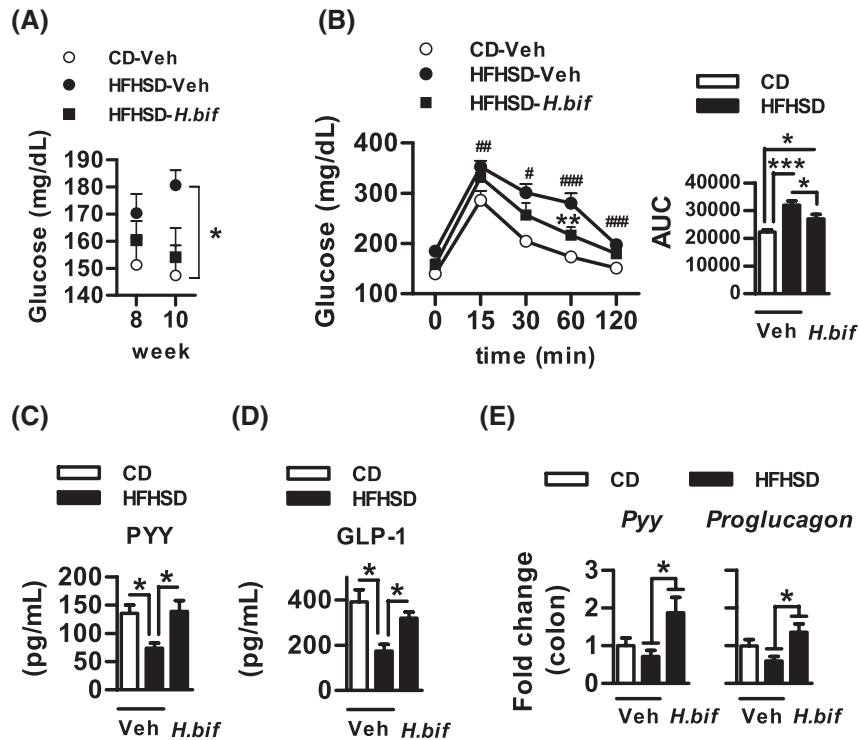


FIGURE 1 *Holdemanella biformis* improves glucose homeostasis and restores the plasma levels of peptide tyrosine tyrosine (PYY) and glucagon like peptide-1 (GLP-1) in diet-induced obese mice independent of body weight. A, Glucose levels in plasma at week 8 and 10 of the study; B, blood glucose levels after 0, 15, 30, 60, and 120 minutes of an oral load of glucose (2 g/kg) to 4-hours fasted mice (oral glucose tolerance test [OGTT]) and area under the curve (AUC) (at week 10 of intervention, n = 9); C, plasma levels of PYY (n = 8-9) and D, GLP-1 (n = 5-6) and E, *pyy* and *proglucagon* expression in colon at the end of the study. Data represent the mean ± SEM. Significant differences were assessed by two-way ANOVA followed by Bonferroni *post hoc* test (body weight and OGTT) or one-way ANOVA followed by Tukey *post hoc* test. #*P* < .05 and ###*P* < .001 versus controls; **P* < .05, ***P* < .01, and ****P* < .001

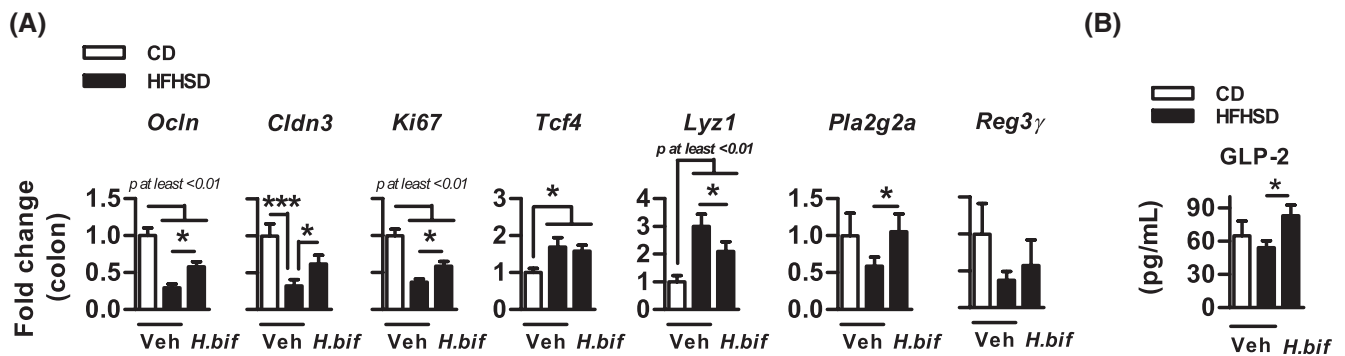


FIGURE 2 *Holdemanella biformis* restores the expression of gut barrier integrity-related markers and increases GLP-2 plasma levels. A, mRNA levels of tight junction protein genes (*Ocln* and *Cldn3*); a proliferation marker (*Ki67*); a Paneth cell differentiation marker (*Tcf4*) and antimicrobial peptide genes (*Lyz1*, *Pla2g2a* and *Reg3γ*) in colon (n = 8) and B, GLP-2 levels in plasma (n = 5-7) at the end of the study. Data represent the mean ± standard error of the mean (SEM). Significant differences were assessed by one-way ANOVA and Tukey *post hoc* test **P* < .05

not shown), pointing to a major contribution of colonic L cells in the elevated circulating levels of PYY and GLP-1. No significant changes in the expression of these genes in the colon or ileum were observed as a consequence of HFHSD-feeding.

Thus, excluding the weight loss confounding effects, these data indicate that *H. biformis* improves systemic glucose homeostasis in obesity and that restoration of PYY and GLP-1 levels might contribute to the metabolic benefits of *H. biformis*.

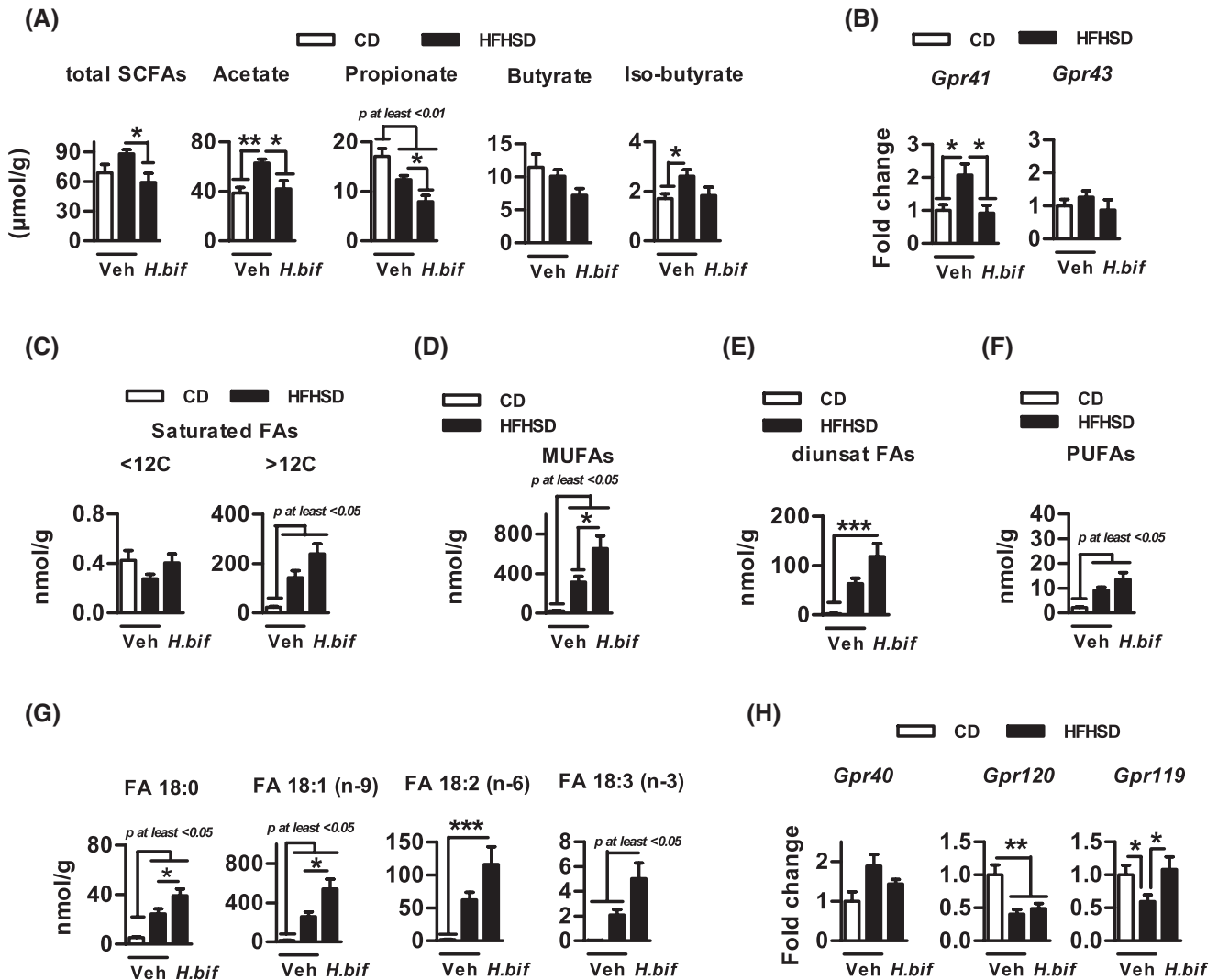


FIGURE 3 *Holdemanella biformis* enhances the concentration of C18 fatty acids in the cecum of diet-induced obese mice. A, total short chain fatty acids (SCFAs), acetate, propionate, butyrate, and isobutyrate concentration ($\mu\text{mol/g}$ of dry weight of cecal content; $n = 9$); B, mRNA levels of *Gpr41* and *Gpr43* in colon ($n = 8$); C, saturated FAs with less or more than 12C (nmol/g of dry weight of cecal content; $n = 9$); D, total MUFAs, E, diunsaturated FAs and F, PUFAs (nmol/g of dry weight of cecal content; $n = 9$); G, C18 FAs (nmol/g of dry weight of cecal content; $n = 9$) and colonic expression of lipid sensing-related receptors (*Gpr40*, *Gpr120* and *Gpr119*, $n = 8$). Data represent the mean \pm standard error of the mean (SEM). Statistical significance was assessed by one-way ANOVA followed by Tukey post hoc test. * $P < .05$, ** $P < .01$, and *** $P < .001$ (see also Figure S1)

3.2 | *Holdemanella biformis* beneficially regulates gut barrier integrity markers and GLP-2 levels

Given that *H. biformis* derived metabolites confer protection to colonic gut barrier against inflammation³¹ which in turn might ameliorate the inflammation-induced metabolic disturbance in obesity, we explored markers of gut barrier integrity and antimicrobial properties in the colon. Gene expression of the tight junction proteins occludin (*Ocln*) and claudin 3 (*Cldn3*), as well as the proliferation marker *Ki67*, was reduced in the colon of HFHSD-fed mice but was partially restored by *H. biformis* (Figure 2A), suggesting that it exerted a protective effect in

gut barrier integrity. Analysis of colon samples showed that expression of T cell-specific transcription factor 4 (*Tcf4*), involved in Paneth cell differentiation, was higher in DIO mice than in CD mice (Figure 2A). Lysozyme 1 (*Lyz1*) expression was also increased, although other antimicrobial peptides such as phospholipase A2 group IIA (*Pla2g2a*) or regenerating islet-derived protein 3 gamma (*Reg3 γ*) tended to be reduced or remained unchanged, respectively (Figure 2A). *Tcf4* mRNA levels remained elevated in the colon of *H. biformis*-treated DIO mice, whereas *Lyz1* or *Pla2g2a* levels tended to be normalized after the intervention. We did not identify changes in immune cells of the intestinal epithelium involved in gut barrier protection and defense processes such as natural and

induced IEL or ILC1 after 13 weeks of *H. biformis* intervention under HFHSD (data not shown).

The plasma levels of the proglucagon-derived hormone GLP-2, which displays protective effects on intestinal integrity, were higher in *H. biformis*-treated mice compared with HFHSD controls (Figure 2B).

Overall, our findings suggest a primary role of *H. biformis* on L cells function, rather than on immunity, that contributes to both gut integrity, through stimulation of GLP-2, and glucose tolerance, through stimulation of PYY and GLP-1 production.

3.3 | *Holdemanella biformis* enhances C18 fatty acid abundance in the cecum of DIO mice

Examination of cecal SCFAs, which act as L cells-stimulating metabolites, in HFHSD-fed mice revealed an increase in the levels of acetate and isobutyrate but a decrease in the levels of propionate (Figure 3A). Acetate and isobutyrate levels were normalized by *H. biformis* administration, but this was significant only for acetate, and propionate levels were lower than in untreated DIO mice (Figure 3A). The colonic expression of the SCFAs receptor gene *Gpr41*, but not *Gpr43*, mirrored the changes in acetate levels, with enhanced expression in untreated DIO mice compared with CD mice and normalized levels in *H. biformis*-treated mice (Figure 3B). Based on this evidence, we could discard SCFAs as the metabolites behind of the effects of *H. biformis* on hormones produced by L cells. We also explored effects on long chain fatty acids (LCFAs) as they act as secretagogues of PYY, GLP-1, and GLP-2. The abundance of cecal saturated LCFAs longer than C12 (Figure 3C) and total monounsaturated and polyunsaturated fatty acids (MUFAs and PUFAs, respectively) was significantly higher in untreated DIO mice than in CD mice (Figure 3D,F). Compared with untreated DIO mice, the administration of *H. biformis* especially enhanced the abundance of total MUFAs (Figure 3D). When exploring different FA molecules, we found that *H. biformis* particularly increased the pre-absorptive abundance of C18 FAs including FA 18:0 (octadecanoic acid), FA 18:1 (n-9) (oleic acid), FA 18:2 (n-6) (linoleic acid), and FA 18:3 (n-3) (α linolenic acid) (Figure 3G). The levels of less abundant FAs are shown in Figure S1. The analysis of lipid sensing G coupled-protein receptors (GPRs) indicated that the increased levels of LCFAs in the cecum were associated with reduced colonic expression of *Gpr120* and *Gpr119* in untreated HFHSD-fed mice (Figure 3H). However, *H. biformis* administration restored the colonic expression of *Gpr119* but not of *Gpr120* (Figure 3H).

3.4 | *Holdemanella biformis* favors the abundance of intestinal bacteria associated with metabolic health which positively correlates with unsaturated long chain fatty acids

We first examined the impact of HFHSD on the gut microbiota by assessing differences in alpha and beta diversity (Figure 4A,B). Regarding alpha diversity, we observed an increase in richness in untreated DIO mice ($P < .018$), supported by the differential distribution of the Chao index and observed operation taxonomic units (OTUs), suggesting the acquisition of new bacterial species (Figure 4A). *H. biformis* administration attenuated the increases in species richness, with values similar to those in CD-fed mice ($P > .110$). The microbial community structure as a whole clearly shifted as a consequence of the HFHSD according to multivariate analysis based on the Bray–Curtis dissimilarity index (PERMANOVA = 10.8, $P = .001$) (Figure 4B). This pattern was not reversed by *H. biformis* administration. Also, HFHSD caused a depletion of several OTUs belonging to the family Muribaculaceae (LDA score = 3.10, $P < .021$), species being predominant in murids (Figure 4C). Conversely, HFHSD increased the abundance of some OTUs belonging to the genera *Bacteroides* (LDA = 3.46, $P = .049$) and *Alistipes* (LDA = 3.47, $P = .008$) and of some species from the families Lachnospiraceae and Ruminococcaceae (LDA > 3.04, $P < .011$) (Figure 4C), and this was attenuated in DIO mice administered *H. biformis*. We also found that *H. biformis* intake increased *Lactobacillus* (LDA = 3.73, $P = .001$) and *Akkermansia* (LDA = 4.88, $P = .045$) species in mice despite their exposure to HFHSD. Additionally, *H. biformis* promoted the growth of the genera *Oscillibacter* (Clostridium cluster IV) (LDA = 3.48, $P = .002$) and *Blautia* (Clostridium cluster XIVa) (LDA = 4.01, $P = .029$).

The phylogenetic tree constructed from multiple sequence alignments of OTUs identified at the genus level as *Faecalibaculum*, the OTU1208 uniquely identified as *Holdemanella* spp., and the V3-V4 regions from the *H. biformis* 16S rRNA gene indicated that OTU1208 likely corresponds to *H. biformis* (Figure S2A), and its presence was only observed in *H. biformis*-treated mice, although this OTU was not detected in all mice (Figure S2B). On the other hand, the OTUs more abundant in the *H. biformis* intervention group, such as those belonging to the genera *Blautia* and *Tyzzelerella*, positively correlated to LCFAs longer than C12, being this correlation stronger with unsaturated FAs, that is, total MUFAs (including oleic acid), diunsaturated FAs, and PUFAs (including α linolenic acid) (Figure 5). By contrast, these genera negatively correlated to saturated FAs shorter than C12 and to butyrate and propionate (Figure 5).

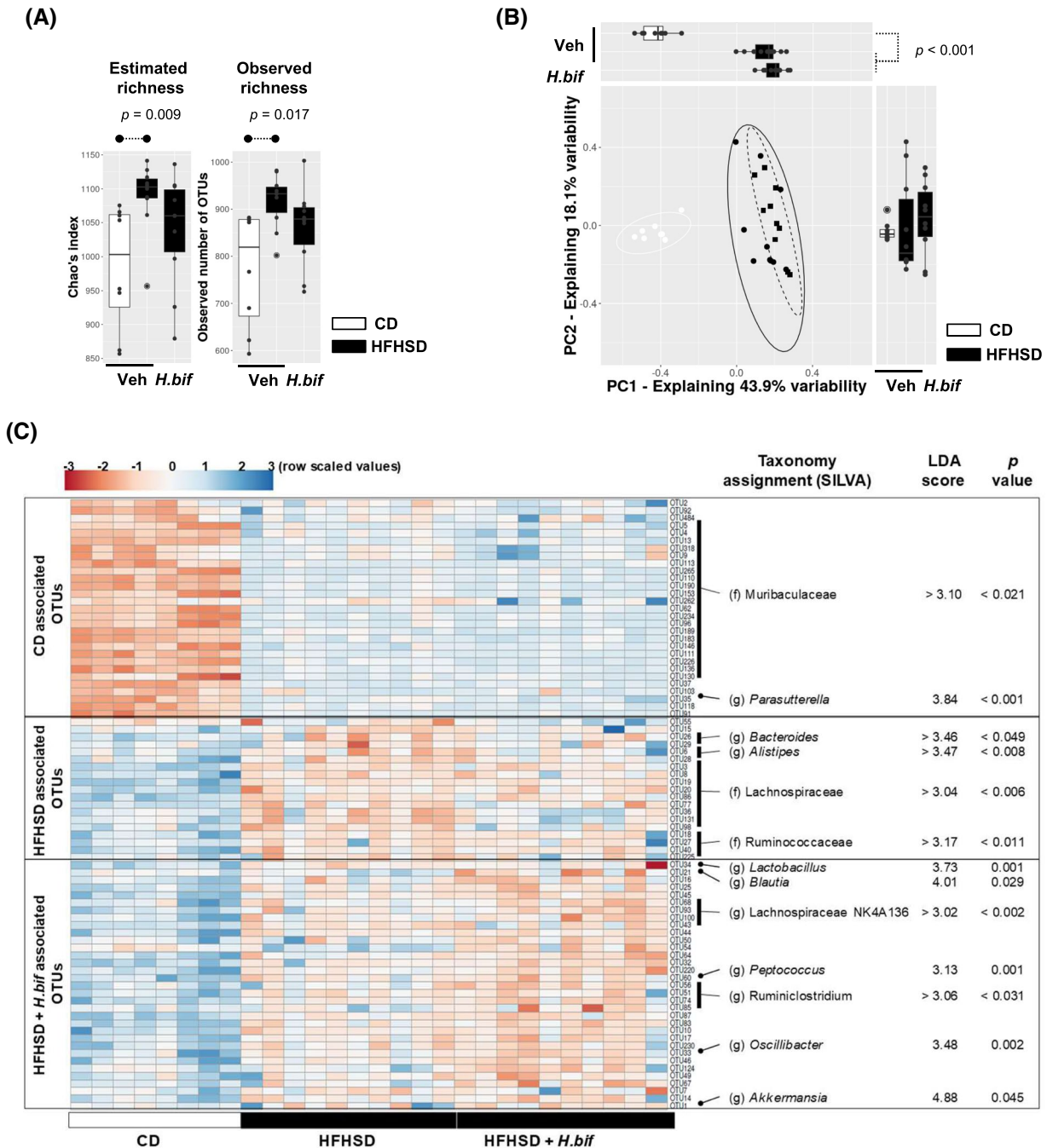
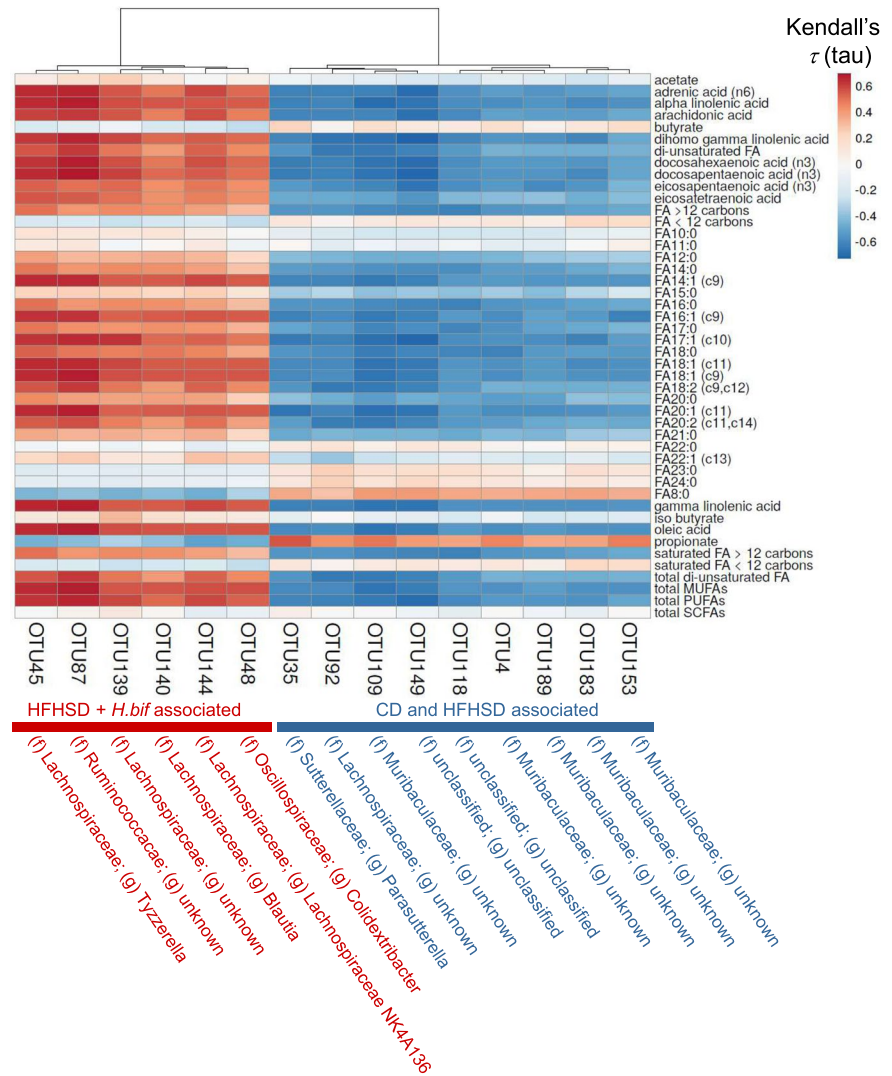


FIGURE 4 *Holdemanella biformis* increases the abundance of bacterial genera associated with metabolic health. A, Richness-based alpha diversity analysis of Operational Taxonomic Units (OTUs) in feces of mice receiving control diet (CD) or high fat high sugar diet (HFHSD) with or without *H. biformis*. *P*-values obtained after pairwise Wilcoxon Rank Sum test (unpaired) with Benjamini–Hochberg post hoc correction are shown on top boxplots when equal or less than 0.05 ($n = 9-10$); B, exploratory analysis based on principal coordinate analysis (PCoA) using Bray–Curtis dissimilarity index. Two main principal coordinates (PC) explaining more than 60% variability are shown in a scatter plot. Marginal boxplots disclose individual distribution of PC values. Differences in PC distribution across group samples were assessed using pairwise Wilcoxon Rank Sum test (unpaired) with Benjamini-Hochberg post hoc correction ($n = 9-10$); C, heatmap compiling profiles for more than 80 OTUs detected to have differential abundance across sample groups (columns). Blue-red scale represents values after raw scaling of normalized DNA read counts. The most accurate taxonomy identification, LDA score and *p*-value resulting from LDA are shown for all OTUs accordingly. Taxonomy for OTUs with uncertain classification at the family, genus, or species level was omitted ($n = 9-10$). Data represent the mean \pm standard error of the mean (SEM) (see also Figure S2)

FIGURE 5 Correlation among microbiota features and cecal lipids. Nonparametric and ranked Kendall correlation (τ parameter) was calculated through pairwise comparisons between the top 166 Operational Taxonomic Units (OTUs) ($\geq 0.05\%$ relative abundance), accounting for $\sim 89\%$ diversity on average, and different fatty acids identified and quantified in cecal samples. Adjusted p -values were obtained by applying the false discovery rate (FDR, q -value) post hoc correction. Correlations with extreme tau values (≥ 0.55 and ≤ -0.55 , q -value < 0.01) were selected to draw the heatmap shown. Few OTUs repeatedly showed multiple meaningful correlations with lipids assessed. The OTU clustering (*Euclidean* distance and *Complete* method) over Kendall's tau values suggests two groups of OTUs differentially associated with fatty acids. OTUs with red labeled taxonomy (f: family, g: genus) show positive correlations with lipid abundance, whereas the OTUs with blue labels show the opposite association. FA: fatty acids, MUFA: mono-unsaturated FA, PUFA: poly-unsaturated FA, SCFA: short-chain FA



3.5 | *Holdemanella biformis* enhances GLP-1 signaling in the small intestine and GLP-1 responsiveness in vagal afferent neurons

Besides the endocrine effects on L cells-produced hormones, we also postulated that *H. biformis*, via its transit through the upper intestine, could modulate lipid sensing routes which can contribute to improve glucose homeostasis as well. Further exploration of potential mediators of *H. biformis*-related benefits in the upper gut was restricted to GLP-1 because of the primary role of this peptide in glucose metabolism and, accordingly, its therapeutic potential to treat T2D.

H. biformis, but not HFHSD alone, increased the expression of the enzyme long-chain acyl-CoA synthetase (*acs13*) and GLP-1 receptor (*Glp-1r*) in the duodenum (Figure 6A), both involved in lipid sensing routes that improve glucose homeostasis through the gut-brain-liver axis. *H. biformis* administration failed to modulate both the *proglucagon* expression in duodenum and the GLP-1 secretory capacity in a human duodenal L cell line (HuTu-80) in vitro (Figure S3). This suggests that the stimulation of GLP-1 secretion by

a direct action of *H. biformis* in duodenal L cells was not the mechanism through which *H. biformis* enhanced duodenal *Glp-1r* signaling. We postulated that the transit of *H. biformis* throughout the upper gut could directly stimulate vagal afferents, densely innervating the duodenum, possibly through bioactive molecules of its cellular wall. Thus, we further explored the potential neuromodulatory properties of *H. biformis* on GLP-1-sensitive neurons involved in the gut-to-brain sensory transmission, to question whether it has the capacity to functionally modulate the central control of meal-related glycemic excursion. We tested this in NG neurons (cell bodies of the visceral afferents) to discriminate the effects of *H. biformis* on the extrinsic intestinal nervous system (vagus nerve) from those induced on the intrinsic nervous system (enteric nervous system).

H. biformis exhibited neuroactive properties on GLP-1-responsive primary cultures of NG neurons, as indicated by the increased neural activity measured as enhanced intracellular Ca^{2+} levels in Fluo4-loaded cells in response to the bacterium (Figure 6B), and the depolarization of RMP (5.69 ± 1.7 mV) in current-clamp recordings, similar to

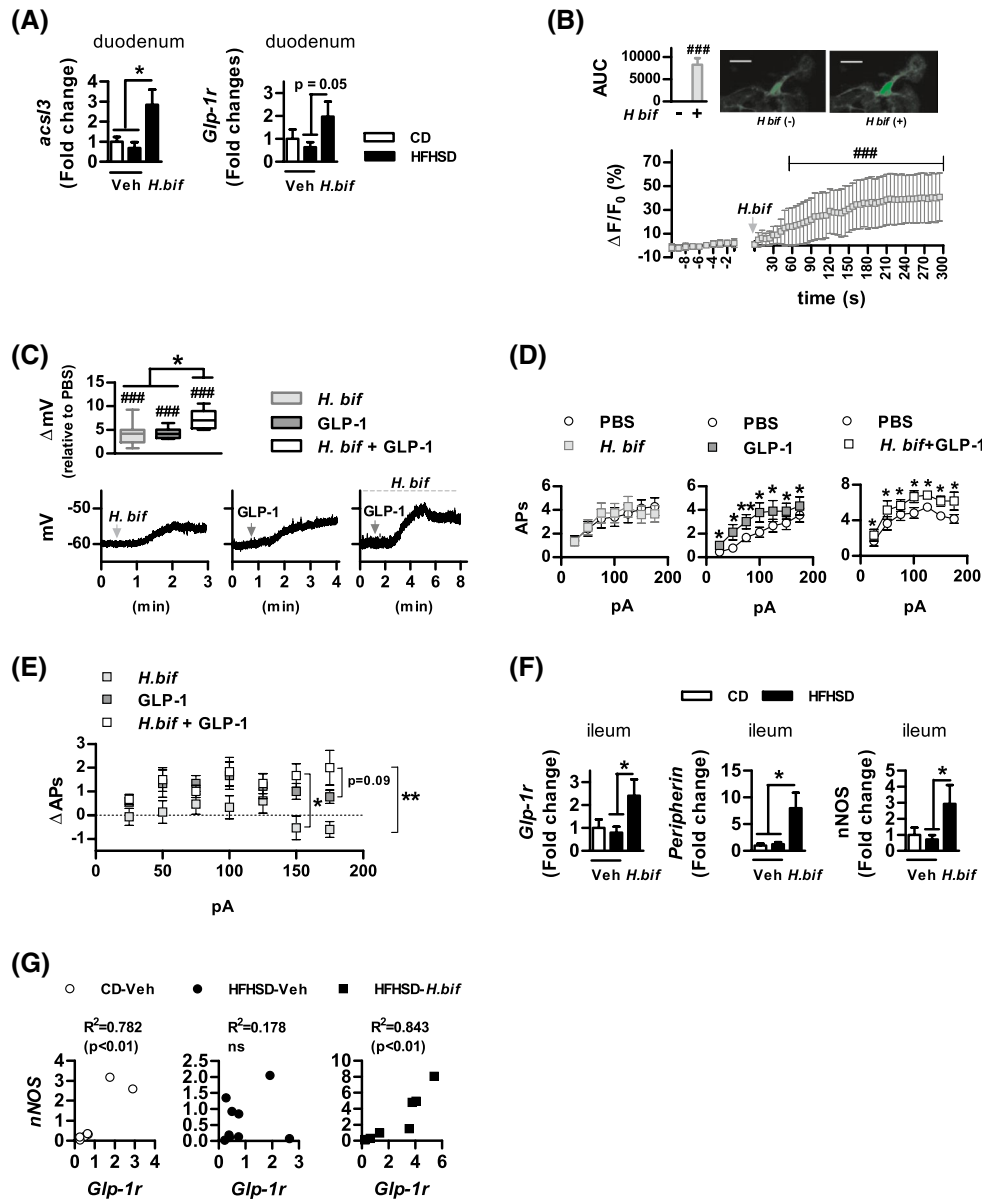


FIGURE 6 *Holdemanella biformis* promotes glucagon like peptide-1 (GLP-1) signaling in small intestine and GLP-1 responsiveness in vagal afferent neurons. A, mRNA levels of *acls3* and *Glp-1r* in duodenum ($n = 8-10$); B, Relative fluorescence intensity ($\Delta F/F_0$) of Fluo-4-preloaded nodose ganglion (NG) cells in response to *H. biformis* ($n = 10$ cells); C–E, perforated whole-cell patch-clamp recordings in NG neurons: C, resting membrane potential (RMP) changes in NG neurons after stimulation with *H. biformis* ($n = 20$ cells), GLP-1 ($n = 8$ cells) or with GLP-1 in *H. biformis*-prestimulated cells ($n = 5$ cells) relative to their respective RMP in response to PBS and representative voltage recording of the RMP changes in response to each treatment; D, number of action potential (APs) fired by NG neurons at different current pulses in presence of *H. biformis* ($n = 15$), GLP-1 ($n = 9$), or GLP-1 after prestimulation with *H. biformis* ($n = 6$); E, difference in the number of fired APs of each treatment relative to PBS; F, *Glp-1r*, *Peripherin*, and *nNOS* expression in ileum ($n = 8-10$); and G, correlation between *Glp-1r* and *nNOS* in ileum ($n = 8$). Data represent the mean \pm standard error of the mean (SEM). Statistical significance was assessed by two-way ANOVA followed by Bonferroni post hoc test (B: stimuli \times time interaction and D: stimuli \times current pulses interaction); one-way ANOVA followed by Tukey post hoc test (A, F), Pearson correlation coefficient (G), repeated measures ANOVA followed by Tukey post hoc test (E), paired Student's *t* test (C) and unpaired Student's *t* test (E). ### $P < .01$ and #### $P < .001$ versus basal condition; * $P < .05$ and ** $P < .01$. Only GLP-1-responding NG cells (9 out of 14) were considered for the perforated whole-cell patch-clamp recordings

that triggered by GLP-1 (4.30 ± 0.4 mV) (Figure 6C). Additionally, prestimulation of NG neurons with *H. biformis* had an additive effect on GLP-1-induced depolarization of the RMP (7.11 ± 0.9 mV) (Figure 6C). GLP-1, but

not *H. biformis*, enhanced AP firing in response to current pulses in NG neurons prestimulated or not with *H. biformis* (Figure 6D). When compared with GLP-1-stimulated cells, no major changes were observed in the GLP-1-related AP

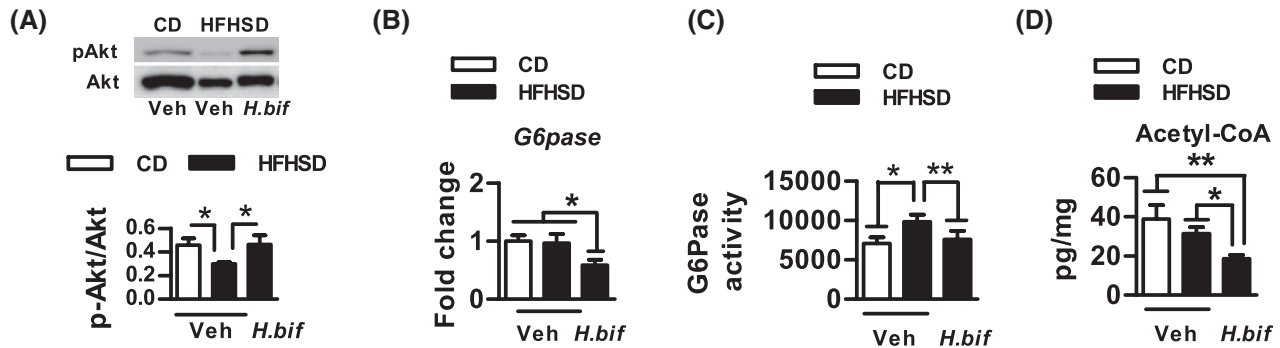


FIGURE 7 *Holdemanella biformis* normalizes insulin sensitivity and gluconeogenesis in the liver of diet-induced obese mice. A, Representative western blot and p-AKT quantification relative to total AKT (n = 8-10); B, mRNA levels of *G6pase* (n = 7-8); C, G6Pase activity (nmol/min/g) (n = 9-10) and D, Acetyl-CoA concentration (n = 9-10). Values were represented as the mean \pm standard error of the mean (SEM). Statistical significance was assessed by one-way ANOVA followed by Tukey post hoc test. * $P < .05$ and ** $P < .01$ (see also Figure S4)

firing pattern in *H. biformis* prestimulated neurons, although there was a tendency for an increased number of APs in response to 175 pA ($P = .09$, Figure 6E).

In ileum, *H. biformis* also increased the expression of *Glp-1r* that remained unchanged in untreated DIO mice (Figure 6F). Ileal expression of *peripherin*, an enteric neuron marker, and *nNOS*, a synthase that produces nitric oxide (NO) in enteric neurons, was also higher after *H. biformis* intervention (Figure 6F). Also, *Glp-1r* and *nNOS* expression positively correlated in CD and *H. biformis*-treated DIO mice but not in untreated DIO mice (Figure 6G). *nNOS* expression in the duodenum was not affected by *H. biformis* (data not shown) which could suggest that the enhancement of *Glp-1r* signaling in upper gut does not trigger a NO upstream signaling in enteric neurons.

Altogether, our findings suggest that *H. biformis* administration enhances GLP-1-mediated neural signaling in the small intestine of DIO mice. Also, we demonstrate in vitro that *H. biformis* stimulates sensory neurons involved in gut-to-brain nutrient signal transmission, which might enhance their sensitivity to GLP-1.

3.6 | *Holdemanella biformis* improves insulin sensitivity and gluconeogenesis in the liver of DIO mice

As *Glp-1r* vagal signaling in the upper gut reduces the hepatic production of glucose,⁴⁸ we explored whether or not the *H. biformis*-related vagal *Glp-1r* signaling in the gut was associated with improved glucose metabolism in liver. Analysis of basal insulin signaling in liver revealed that DIO mice had a significantly lower level of AKT phosphorylation than CD mice, and this was restored by *H. biformis* administration (Figure 7A). The glycogen content was normal in untreated and *H. biformis*-treated DIO mice (data not shown). Further gene expression analysis in liver showed that phosphoenolpyruvate carboxykinase 1 (*Pck1*) (data not shown) and

glucose-6-phosphatase (*G6Pase*) (Figure 7B), rate-limiting enzymes of gluconeogenesis, were unaffected by HFHSD. By contrast, the administration of *H. biformis* in DIO mice led to a decrease in liver *G6pase* levels (Figure 7B), but *Pck1* were unaffected (data not shown). Despite the unaffected *G6pase* gene expression, DIO enhanced hepatic G6Pase activity, which was normalized by *H. biformis* (Figure 7C). Hepatic levels of acetyl-CoA, an allosteric metabolite that enhances gluconeogenesis, were lower in *H. biformis*-treated DIO mice than in untreated DIO mice or controls (Figure 7D). The exploration of central mechanisms involved in the hepatic glucose production revealed a downregulation of *Npy* and *AgRP* gene expression in the hypothalamus of untreated and *H. biformis*-treated DIO mice (Figure S4); also, the *pmc* expression tended to increase in untreated DIO mice but not in mice receiving *H. biformis* and the *Cart* expression remained unaffected whatever the treatment (Figure S4).

4 | DISCUSSION

Herein, we show that *H. biformis*, an intestinal bacterium isolated from a metabolically healthy human subject, has antidiabetic effects in a rodent model of DIO. *H. biformis* administration reduced fasting glucose levels and improved oral glucose tolerance in DIO mice, but it failed to alleviate body weight gain and plasma markers of lipid metabolism such as cholesterol. These data indicate that *H. biformis* specifically regulates glucose homeostasis and that this is not a consequence of the common weight loss-associated metabolic benefits.

In particular, *H. biformis* restored the plasma levels of PYY and GLP-1 in DIO mice, suggesting that it plays a primary role in modulating the enteroendocrine L cells and, thus, enhances the endocrine-mediated gluoregulatory actions of these gut hormones. We also found that *H. biformis* exerted these effects in the large rather than the small intestine, since it increased *pyy* and *proglucagon* transcription in

colon, but not in the ileum, an intestinal region which could also contribute to improving glucose homeostasis.⁴⁹

Moreover, *H. biformis* supplementation increased LCFAs in the cecum, especially C18 unsaturated FAs, which strongly stimulate the secretion of gut hormones from L cells compared with other LCFAs.⁵⁰ This increase in the pre-absorptive levels of C18 FAs could be the mechanism by which *H. biformis* triggered the release of PYY, GLP-1, and GLP-2 in the distal gut, especially through the stimulatory action of FA 18:1 (n-9) (oleic acid) and FA 18:3 (n-3) (α linolenic acid) on L cells.^{33,51,52} Partly in line with our findings, previous studies have shown that *H. biformis* displays anti-inflammatory and antitumorigenic effects through both SCFAs and LCFAs production,^{30,31} which are also PYY and GLP-1 secretagogues.⁵³

H. biformis could contribute to increasing the levels of oleic and α linolenic acid through its own capacity to produce C18 FAs,³¹ amplifying some of the HFHSD-associated effects. Furthermore, *H. biformis*-induced changes in gut microbiota composition might also account for changes in intraluminal LCFAs metabolism. Based on the correlations identified between the gut microbiota and cecal lipidome, we hypothesize that *H. biformis*-intervention would favor FA elongation through a process where SCFAs would prime the synthesis of FA longer than C12 (LCFAs), via condensation of acetate units (acetyl-CoA) and additional SCFAs interconversions.⁵⁴ Furthermore, SCFAs-producing species of the genera *Tyzzarella* and *Blautia* might also be involved in this process. In addition, the restoration of the colonic expression of *Gpr119* along with the increased LCFAs derivatives, such as oleoylethanolamide, N-linoleylethanolamine or oleoylglycerol, which are GPR119 ligands, could contribute to restoring the circulating levels of gut hormones in *H. biformis*-treated DIO mice.^{23,55,56} In the DIO model, we also identified a GLP-2-mediated mechanism potentially involved in the capacity of *H. biformis* to strengthen the gut barrier function, as indicated by the expression of certain markers of gut integrity.^{50,57} The effects of *H. biformis* could be due not only to the stimulation of GLP-2 secretion but also to secondary changes in the microbial ecosystem, characterized by increases in *Akkermansia* spp., which are also reported to strengthen the gut barrier integrity in preclinical models of obesity.²³ Nonetheless, we did not detect effects of the *H. biformis*-intervention on immune cells located in the intestinal epithelium primarily involved in the intestinal barrier defenses, such as IEL and ILC1. Overall, the findings highlight the specificity of our *H. biformis* strain to act on the enteroendocrine system rather than on the immune system.

Glucose homeostasis is also maintained by lipid sensing pathways in the small intestine.⁵⁸ Postprandial glycemia and hepatic glucose production is reduced by the stimulation of lipid sensing routes triggered by diverse signals, including the enzyme ACSL3 and the GLP-1 receptor,^{48,59} whose

expression was boosted by *H. biformis* in the duodenum. Thus, in addition to favoring the endocrine actions of gut hormones from colonic L cells, *H. biformis* also enhanced lipid-signaling routes in the upper gut, which can improve glucose homeostasis independently of the circulating levels of these hormones.

Studies in rodents revealed that *acs3* expression in the duodenum is dependent on gut microbiota composition and bile acids⁵⁹ and that the reduced glucose production via GLP-1 receptor neural signaling is triggered by duodenal infusion of oleic and linoleic acid.^{48,59} Although future research should be conducted to identify the precise mechanisms by which *H. biformis* activates ACSL3 and GLP-1 receptor-mediated lipid sensing routes, we suggest that changes on the gut microbiota composition and in the composition and/or secretion of bile acids could impact on FAs digestion and absorption. In turn, this would influence the intraluminal availability of bioactive lipids able to improve glucose homeostasis through endocrine and paracrine routes.

Since *H. biformis* did not directly influence the L cell secretory capacity in vitro, we also consider that this bacterial species may directly stimulate gut-to-brain neural sensory pathways to control energy homeostasis, as previously described for other bacterial bioactive molecules such as muramyl dipeptide and lipopolysaccharide.¹⁰ Here we demonstrated that likely through a neuroactive cell wall component(s), *H. biformis* directly depolarized NG neurons, which receive sensory information from the extrinsic primary neurons of the gut to be transmitted to the brain, and increased their GLP-1 responsiveness. Although further investigation should identify the *H. biformis*-derived neuroactive molecules and discover whether they can reach vagal afferents in the lamina propria, our in vitro experiments provide a proof-of-concept of the potential role played by *H. biformis* in stimulating the gut–brain axis through a GLP-1-mediated vagal afferent mechanism. In fact, previous research has revealed the importance of GLP-1 signaling in NG neurons to maintain postmeal glycemia and insulin release.¹³

The gut–brain axis is also stimulated in the ileum by GLP-1 through paracrine actions on enteric neurons, whereby receptor activation stimulates nNOS and nitric oxide (NO)-mediated neurotransmission to control gastric emptying and insulin secretion.¹⁰ These routes are impaired in mice under hypercaloric diets as a result of the altered gut microbiota structure and function.¹⁰ Our study also shows that *H. biformis* upregulates the transcription of *Glp-1r*, *peripherin*, and *nNOS*, but future research must clarify whether or not these transcriptional changes are functionally translated into NO neurotransmission through the gut–brain axis, as well as identify the underlying microbiota-related players.

In addition of improving oral glucose tolerance, *H. biformis* restored insulin signaling and reduced gluconeogenesis in liver. There is growing evidence that circulating

GLP-1 influences hepatic glucose metabolism through central signaling, independently of the incretin effect, rather than through a direct effect on liver, as there is no robust evidence for GLP-1 receptor expression in hepatocytes.⁶⁰ Thus, *H. biformis*-associated hepatic gluco regulatory effects might be a consequence of the vagal-mediated modulation of the gut-brain-liver axis. Indeed, the vagal efferent outflow stimulated by gut lipid sensing is reported crucial to reduce glucose production and improve insulin sensitivity in the liver but not in adipose tissue or muscle.⁴⁸

Although our results suggest that *H. biformis* modulates the gut-brain-liver axis to improve glucose homeostasis, further investigations should be conducted to explore whether these findings, observed in basal condition, also occur postprandially (after a meal). Such studies should also explore the gluco regulatory effects mediated by PYY, GLP-1, and GLP-2 via endocrine actions and by GLP-1 via paracrine signaling on the gut-brain-liver axis.

Taken together, our study shows that *H. biformis* improves glucose tolerance independent of obesity, impacting mainly on different aspects of the GLP-1 signaling pathway. First, *H. biformis* increases the expression of the GLP-1 precursor (*proglucagon*) in the colon and the hormone concentration in circulation, likely as a result of secondary changes in intestinal metabolites and bacteria. Second, *H. biformis* administration enhances GLP-1 sensitivity and signaling through endocrine and neural circuits, at least partly through direct host-microbe interactions in the duodenum and ileum. Third, the effects of *H. biformis* administration on glucose homeostasis are not limited to the GLP-1 system but might also be a consequence of increases in other endocrine peptides (PYY, GLP-2) as well as of secondary effects on the gut barrier integrity. Of special interest are, however, the effects of this bacterial strain on GLP-1 sensitivity, which could help to boost the efficacy of GLP-1-based therapies in patients with T2D.

ACKNOWLEDGMENTS

The authors thank Isabel Campillo Nuevo and Inmaculada Noguera for technical assistance. This study received funding from the European Union Horizon 2020 research and innovation program under the Marie Skłodowska-Curie grant agreement No. 797297 (M.R-P), from the European Union 7th Framework Program through the *MyNewGut* project (Grant agreement No. 613979) and from the Spanish Ministry of Science and Innovation (MICINN, Spain) (Grant AGL2017-88801-P). The FPI grant of I.L-A from the Ministry of Science and Innovation (MICINN; Spain) and the contract of C. B-V for promotion of youth employment in R+D+I from MICINN (Spain) are fully acknowledged.

CONFLICT OF INTEREST

The authors declare no competing interests.


AUTHOR CONTRIBUTIONS

Conceptualization: M.R-P, I.L-A, A.J.L, and Y.S; Methodology: M.R-P, I.L-A, C.B-V, L.R-R, E.M.G, A.B-P, G.L; Investigation: M.R-P, I.L-A, C.B-V, L.R-R, E.M.G, A.B-P, and G.L; Writing—Original Draft: I.L-A, M.R-P; Writing—Review & Editing: A.J.L and Y.S; Funding Acquisition: Y.S; Resources: A.J.L and Y.S; Supervision: Y.S.

DATA AVAILABILITY STATEMENT

The files containing fastq raw data can be publicly accessed at the European Nucleotide Archive (ENA) via bioproject number PRJEB38356. Partial 16S rRNA gene sequence from *Holdemanella biformis* G59 can be accessed at the ENA via OD916885 accession number.

ORCID


Marina Romaní-Pérez  <https://orcid.org/0000-0002-1009-0156>

Inmaculada López-Almela  <https://orcid.org/0000-0001-9886-8622>

Clara Bullich-Vilarrubias  <https://orcid.org/0000-0002-4352-0810>

Lola Rueda-Ruzafa  <https://orcid.org/0000-0002-0151-8018>

Eva M. Gómez Del Pulgar  <https://orcid.org/0000-0002-4509-1044>

Alfonso Benítez-Páez  <https://orcid.org/0000-0001-5707-4340>

José Antonio Lamas  <https://orcid.org/0000-0002-4453-4595>

Yolanda Sanz  <https://orcid.org/0000-0002-1615-1976>

REFERENCES

- Ley RE, Turnbaugh PJ, Klein S, Gordon JI. Microbial ecology: human gut microbes associated with obesity. *Nature*. 2006;444:1022-1023.
- Turnbaugh PJ, Hamady M, Yatsunenkov T, et al. A core gut microbiome in obese and lean twins. *Nature*. 2009;457:480-484.
- Ridaura VK, Faith JJ, Rey FE, et al. Gut microbiota from twins discordant for obesity modulate metabolism in mice. *Science*. 2013;341:1241-1244.
- Carmody RN, Gerber GK, Luevano JM, et al. Diet dominates host genotype in shaping the murine gut microbiota. *Cell Host Microbe*. 2015;17:72-84.
- David LA, Maurice CF, Carmody RN, et al. Diet rapidly and reproducibly alters the human gut microbiome. *Nature*. 2014;505:559-563.
- Fung TC, Olson CA, Hsiao EY. Interactions between the microbiota, immune and nervous systems in health and disease. *Nat Neurosci*. 2017;20:145-155.
- Martin CR, Osadchiy V, Kalani A, Mayer EA. The brain-gut-microbiome axis. *Cell Mol Gastroenterol Hepatol*. 2018;6:133-148.
- Christ A, Lauterbach M, Latz E. Western diet and the immune system: an inflammatory connection. *Immunity*. 2019;51:794-811.

9. Garidou L, Pomié C, Klopp P, et al. The gut microbiota regulates intestinal CD4 T cells expressing ROR γ t and controls metabolic disease. *Cell Metab.* 2015;22:100-112.
10. Grasset E, Puel A, Charpentier J, et al. A specific gut microbiota dysbiosis of Type 2 diabetic mice induces GLP-1 resistance through an enteric NO-dependent and gut-brain axis mechanism. *Cell Metab.* 2017;25:1075-1090.e5.
11. Wollam J, Riopel M, Xu Y-J, et al. Microbiota-produced N-formyl peptide fMLF promotes obesity-induced glucose intolerance. *Diabetes.* 2019;68:1415-1426.
12. Drucker DJ. Mechanisms of action and therapeutic application of glucagon-like peptide-1. *Cell Metab.* 2018;27:740-756.
13. Krieger J-P, Arnold M, Pettersen KG, Lommel P, Langhans W, Lee SJ. Knockdown of GLP-1 receptors in vagal afferents affects normal food intake and glycaemia. *Diabetes.* 2016;65:34-43.
14. Sandoval DA, Bagnol D, Woods SC, D'Alessio DA, Seeley RJ. Arcuate glucagon-like peptide 1 receptors regulate glucose homeostasis but not food intake. *Diabetes.* 2008;57:2046-2054.
15. Breton J, Tennoune N, Lucas N, et al. Gut commensal *E coli* proteins activate host satiety pathways following nutrient-induced bacterial growth. *Cell Metab.* 2016;23:324-334.
16. Chimere C, Emery E, Summers DK, Keyser U, Gribble FM, Reimann F. Bacterial metabolite indole modulates incretin secretion from intestinal enteroendocrine L cells. *Cell Rep.* 2014;9:1202-1208.
17. Natividad JM, Agus A, Planchais J, et al. Impaired aryl hydrocarbon receptor ligand production by the gut microbiota is a key factor in metabolic syndrome. *Cell Metab.* 2018;28:737-749.e4.
18. Claus SP. Will gut microbiota help design the next generation of GLP-1-based therapies for Type 2 diabetes? *Cell Metab.* 2017;26:6-7.
19. O'Toole PW, Paoli M. The contribution of microbial biotechnology to sustainable development goals: microbiome therapies. *Microb Biotechnol.* 2017;10:1066-1069.
20. Romani-Pérez M, Agusti A, Sanz Y. Innovation in microbiome-based strategies for promoting metabolic health. *Curr Opin Clin Nutr Metab Care.* 2017;20:484-491.
21. Tsai Y-L, Lin T-L, Chang C-J, et al. Probiotics, prebiotics and amelioration of diseases. *J Biomed Sci.* 2019;26:3.
22. Depommier C, Everard A, Druart C, et al. Supplementation with *Akkermansia muciniphila* in overweight and obese human volunteers: a proof-of-concept exploratory study. *Nat Med.* 2019;25:1096-1103.
23. Everard A, Belzer C, Geurts L, et al. Cross-talk between *Akkermansia muciniphila* and intestinal epithelium controls diet-induced obesity. *Proc Natl Acad Sci USA.* 2013;110:9066-9071.
24. Gauffin Cano P, Santacruz A, Moya Á, Sanz Y. Bacteroides uniformis CECT 7771 ameliorates metabolic and immunological dysfunction in mice with high-fat-diet induced obesity. *PLoS One.* 2012;7:e41079.
25. Plovier H, Everard A, Druart C, et al. A purified membrane protein from *Akkermansia muciniphila* or the pasteurized bacterium improves metabolism in obese and diabetic mice. *Nat Med.* 2017;23:107-113.
26. Rastelli M, Cani PD, Knauf C. The gut microbiome influences host endocrine functions. *Endocr Rev.* 2019;40:1271-1284.
27. Modasia A, Parker A, Jones E, et al. Regulation of enteroendocrine cell networks by the major human gut symbiont *Bacteroides thetaiotaomicron*. *Front Microbiol.* 2020;11. <https://doi.org/10.3389/fmicb.2020.575595>
28. Collins MD, Lawson PA, Willems A, et al. The phylogeny of the genus clostridium: proposal of five new genera and eleven new species combinations. *Int J Syst Evol Microbiol.* 1994;44:812-826.
29. De Maesschalck C, Van Immerseel F, Eeckhaut V, et al. 1977), *Eubacterium bifforme* (Eggerth 1935) and *Eubacterium cylindroides* (Cato et al. 1974) as *Faecalicoccus pleomorphus* comb. nov., *Holdemanella biformis* gen. nov., comb. nov. and *Faecalitalea cylindroides* gen. nov., comb. nov., respectively, within the family Erysipelotrichaceae. *Int J Syst Evol Microbiol.* 2014;64:3877-3884.
30. Zagato E, Pozzi C, Bertocchi A, et al. Endogenous murine microbiota member *Faecalibaculum rodentium* and its human homologue protect from intestinal tumour growth. *Nat Microbiol.* 2020;5:511-524.
31. Pujo J, Petitfils C, Faouder PL, et al. Bacteria-derived long chain fatty acid exhibits anti-inflammatory properties in colitis. *Gut.* 2021;70(6):1088-1097. <https://doi.org/10.1136/gutjn1-2020-321173>
32. Tolhurst G, Heffron H, Lam YS, et al. Short-chain fatty acids stimulate glucagon-like peptide-1 secretion via the G-protein-coupled receptor FFAR2. *Diabetes.* 2012;61:364-371.
33. Hirasawa A, Tsumaya K, Awaji T, et al. Free fatty acids regulate gut incretin glucagon-like peptide-1 secretion through GPR120. *Nat Med.* 2005;11:90-94.
34. Liebisch G, Ecker J, Roth S, et al. Quantification of fecal short chain fatty acids by liquid chromatography tandem mass spectrometry-investigation of pre-analytic stability. *Biomolecules.* 2019;9(4):121. <https://doi.org/10.3390/biom9040121>
35. Ecker J, Scherer M, Schmitz G, Liebisch G. A rapid GC-MS method for quantification of positional and geometric isomers of fatty acid methyl esters. *J Chromatogr B Analyt Technol Biomed Life Sci.* 2012;897:98-104.
36. Klindworth A, Pruesse E, Schweer T, et al. Evaluation of general 16S ribosomal RNA gene PCR primers for classical and next-generation sequencing-based diversity studies. *Nucleic Acids Res.* 2013;41:e1.
37. Magoč T, Salzberg SL. FLASH: fast length adjustment of short reads to improve genome assemblies. *Bioinforma Oxf Engl.* 2011;27:2957-2963.
38. Caporaso JG, Kuczynski J, Stombaugh J, et al. QIIME allows analysis of high-throughput community sequencing data. *Nat Methods.* 2010;7:335-336.
39. Schloss PD, Westcott SL, Ryabin T, et al. Introducing mothur: open-source, platform-independent, community-supported software for describing and comparing microbial communities. *Appl Environ Microbiol.* 2009;75:7537-7541.
40. Edgar RC, Haas BJ, Clemente JC, Quince C, Knight R. UCHIME improves sensitivity and speed of chimera detection. *Bioinforma Oxf Engl.* 2011;27:2194-2200.
41. Quast C, Pruesse E, Yilmaz P, et al. The SILVA ribosomal RNA gene database project: improved data processing and web-based tools. *Nucleic Acids Res.* 2013;41:D590-596.
42. Edgar RC. Search and clustering orders of magnitude faster than BLAST. *Bioinforma Oxf Engl.* 2010;26:2460-2461.
43. Pruesse E, Peplies J, Glöckner FO. SINA: accurate high-throughput multiple sequence alignment of ribosomal RNA genes. *Bioinforma Oxf Engl.* 2012;28:1823-1829.
44. Price MN, Dehal PS, Arkin AP. FastTree: computing large minimum evolution trees with profiles instead of a distance matrix. *Mol Biol Evol.* 2009;26:1641-1650.

45. Letunic I, Bork P. Interactive Tree Of Life (iTOL) v4: recent updates and new developments. *Nucleic Acids Res.* 2019;47:W256-W259.
46. Cadaveira-Mosquera A, Pérez M, Reboreda A, Rivas-Ramírez P, Fernández-Fernández D, Lamas JA. Expression of K2P channels in sensory and motor neurons of the autonomic nervous system. *J Mol Neurosci MN.* 2012;48:86-96.
47. Segata N, Izard J, Waldron L, et al. Metagenomic biomarker discovery and explanation. *Genome Biol.* 2011;12:R60.
48. Yang M, Wang J, Wu S, et al. Duodenal GLP-1 signaling regulates hepatic glucose production through a PKC- δ -dependent neurocircuitry. *Cell Death Dis.* 2017;8:e2609.
49. Lewis JE, Miedzybrodzka EL, Foreman RE, et al. Selective stimulation of colonic L cells improves metabolic outcomes in mice. *Diabetologia.* 2020;63:1396-1407.
50. Brubaker PL. Glucagon-like peptide-2 and the regulation of intestinal growth and function. *Compr Physiol.* 2018;8:1185-1210.
51. Iakoubov R, Ahmed A, Lauffer LM, Bazinet RP, Brubaker PL. Essential role for protein kinase C ζ in oleic acid-induced glucagon-like peptide-1 secretion in vivo in the rat. *Endocrinology.* 2011;152:1244-1252.
52. Rocca AS, LaGreca J, Kalitsky J, Brubaker PL. Monounsaturated fatty acid diets improve glycemic tolerance through increased secretion of glucagon-like peptide-1. *Endocrinology.* 2001;142:1148-1155.
53. Duca FA, Sakar Y, Covasa M. The modulatory role of high fat feeding on gastrointestinal signals in obesity. *J Nutr Biochem.* 2013;24:1663-1677.
54. Boets E, Gomand SV, Deroover L, et al. Systemic availability and metabolism of colonic-derived short-chain fatty acids in healthy subjects: a stable isotope study. *J Physiol.* 2017;595:541-555.
55. Lauffer LM, Iakoubov R, Brubaker PL. GPR119 is essential for oleoylethanolamide-induced glucagon-like peptide-1 secretion from the intestinal enteroendocrine L-cell. *Diabetes.* 2009;58:1058-1066.
56. Cheng Y-H, Ho M-S, Huang W-T, Chou Y-T, King K. Modulation of glucagon-like peptide-1 (GLP-1) potency by endocannabinoid-like lipids represents a novel mode of regulating GLP-1 receptor signaling. *J Biol Chem.* 2015;290:14302-14313.
57. Cani PD, Possemiers S, Van de Wiele T, et al. Changes in gut microbiota control inflammation in obese mice through a mechanism involving GLP-2-driven improvement of gut permeability. *Gut.* 2009;58:1091-1103.
58. Duca FA, Waise TMZ, Peppler WT, Lam TKT. The metabolic impact of small intestinal nutrient sensing. *Nat Commun.* 2021;12:903.
59. Bauer PV, Duca FA, Waise TMZ, et al. *Lactobacillus gasseri* in the upper small intestine impacts an ACSL3-dependent fatty acid-sensing pathway regulating whole-body glucose homeostasis. *Cell Metab.* 2018;27:572-587.e6.
60. Sandoval D, Sisley SR. Brain GLP-1 and insulin sensitivity. *Mol Cell Endocrinol.* 2015;418(Pt 1):27-32.

SUPPORTING INFORMATION

Additional Supporting Information may be found online in the Supporting Information section.

How to cite this article: Romaní-Pérez M, López-Almela I, Bullich-Vilarrubias C, et al. *Holdemanella biformis* improves glucose tolerance and regulates GLP-1 signaling in obese mice. *The FASEB Journal.* 2021;35:e21734. <https://doi.org/10.1096/fj.20210126R>